Chemical Enhancement Effects in SERS Spectra: A Quantum Chemical Study of Pyridine Interacting with Copper, Silver, Gold and Platinum Metals

De-Yin Wu,*,† Xiu-Min Liu,† Sai Duan,† Xin Xu,‡ Bin Ren,‡ Sheng-Hisen Lin,§ and Zhong-Qun Tian‡

Department of Chemistry, College of Chemistry and Chemical Engineering, Xiamen University, Xiamen 361005, Fujian, People Republic of China, State Key Laboratory of Physical Chemistry of Solid Surfaces, Xiamen University, Xiamen 361005, Fujian, China, and Institute of Atomic and Molecular Sciences, Academic Sinica, P. O. Box 23-166, 106 Taipei, Taiwan, China

Received: July 31, 2007

Using density functional theory, we have studied the interactions between pyridine (Py) and coinage metals (silver, copper, and gold) as well as the transition metal platinum. We present here a detailed analysis of the influence of chemical enhancement effects on the SERS signals. We analyze the differential Raman scattering cross sections of the a_1 vibrational modes related to Py. The results show that the relative Raman intensities of SERS spectra depend strongly on the binding interaction between Py and the SERS active centers, the electronic property of metal materials, and the incident wavelengths. When the bonding between Py and a SERS site is very weak, analogous to physical adsorption, the Raman spectra of the adsorbed Py are similar to that of free Py. For Py interacting strongly with copper, gold, and platinum clusters, we find that the Raman intensities of the υ_1, υ_{6a}, υ_{9a}, and υ_{8a} modes of Py are enhanced, whereas the intensity of the υ_{12} mode decreases. To check the enhancement effect of the charge-transfer mechanism, we calculate the preresonance Raman spectra. For Py interacting with silver, copper, and gold clusters, the low-lying charge transfer states are formed from the valence shell s orbital of metal to the unoccupied π*-type orbitals (b_1 and a_2) of the Py ring; whereas for Py adsorbed on platinum clusters, the low-lying charge transfer states are formed due to the transitions from some d orbitals of the metal clusters to the two unoccupied π*-type orbitals of Py. The results show that the Raman spectral property depends strongly on the property of these excited states and the electronic structures of the metal materials.

Introduction

Surface-enhanced Raman scattering (SERS) is one of the most sensitive spectroscopic techniques for detecting surface species and for studying adsorption on metal surfaces. The spectral sensitivity is due to the great enhancement effects, which can amount to as much as several orders in magnitude with respect to that of molecules in bulk[1−3] or even up to 10^{14} fold as found in the single-molecule SERS.[4,5] This giant enhancement arises mainly from two mechanisms, electromagnetic field enhancement (EM) and chemical enhancement (CE). A number of metals have been suggested as being capable of producing SERS. These include silver, gold, copper, nickel, iron, cobalt, platinum, palladium, etc.[6,7] Strong SERS enhancements, due to the EM mechanism, are expected for the metals with shells of $(n-1)d^{10}ns^1$; this is also true for other metals with valence shells of $(n-1)d^m ns^l$ ($0 < m < 10$ and $0 < l < 2$). For the latter, the EM effect is strongly damped due to interband transitions.[2,8] It is worthy of noting that the EM enhancement is originated from the collective excitation of delocalized electrons in metal surfaces and gives rise to the same enhancement effect on the same symmetric modes of adsorbed molecules according to the surface selection rule.[2,7,8] Therefore, for some vibrations with the same irreducible representation, the CE effect should be considered as the main factor to influence their relative Raman intensities, whereas the EM enhancement only magnifies the CE effect on their SERS signals.

Ever since the pioneering work on SERS in the mid-1970s, pyridine (Py), as a surface sensitive probe molecule, has been studied extensively on various metal surfaces with different excitation wavelengths.[6,8−11] The adsorption orientation of Py was suggested to be upright or slightly tilted by the N-end of Py when the surface concentration reaches a monolayer. It has been widely accepted that pyridine molecules, adsorbed on properly roughened metal surfaces, exhibit a remarkable enhancement arising from both EM and CE enhancements.[7,8,10,11] Good quality SERS spectra can easily be observed from coinage metal (silver, gold, and copper) surfaces due to the significant EM enhancement by the highly effective surface plasmon resonance.[10,12,13] From these SERS spectra, there are five intense peaks at 624, 1010, 1035, 1218, and 1598 cm^{-1}, which can be assigned to the totally symmetric modes (a_1) under a C_{2V} point group, asymmetric ring deformation (υ_{6a}, the Wilson notation), ring breathing mode (υ_1), symmetric ring deformation mode (υ_{12}), C−H in-plane bending mode (υ_{9a}), and ring C−C stretching mode (υ_{8a}), respectively.[14] In contrast to the SERS spectra, υ_1 and υ_{12} modes are the only strong normal Raman signals among all of the fundamental modes in the gas-phase Py or pure-liquid Py.[15,16] For these modes, the SERS electro-

* To whom correspondence should be addressed. E-mail: dywu@xmu.edu.cn.

† Department of Chemistry, College of Chemistry and Chemical Engineering, Xiamen University.

‡ State Key Laboratory of Physical Chemistry of Solid Surfaces, Xiamen University.

§ Institute of Atomic and Molecular Sciences, Academic Sinica.

10.1021/jp0760962 CCC: $40.75
Published on Web 02/28/2008

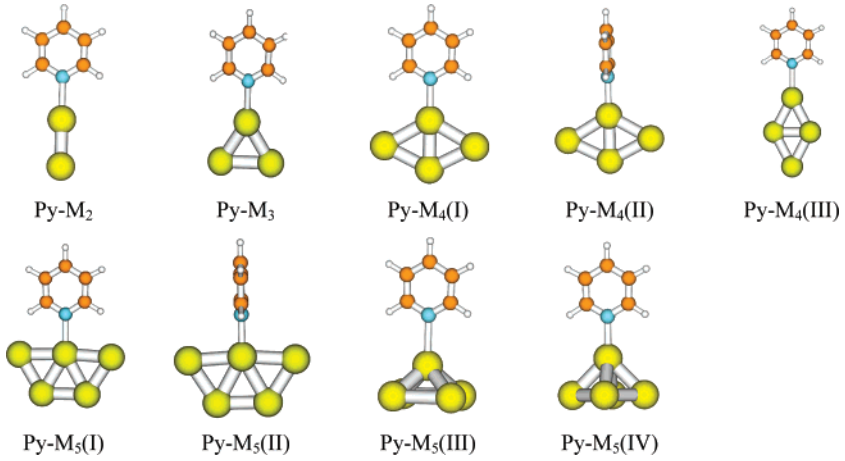

Figure 1. Modeling Structures and Optimized Geometries for Py−M_n (n = 2−5 for M = Cu, Ag, Au; n = 5 for M = Pt) complexes. Note that for Py−Pt_5 complexes only two configurations of Py−Pt_5(III) and Py−Pt_5(IV) were considered here, because the platinum clusters preferred to adopt a 3D structure.

magnetic selection rule is not expected to provide an interpretation on the changes of their relative intensities.[2,7,8,17,18] As mentioned above, it is the CE mechanism that is responsible for the change in the relative Raman intensities.

For transition-metal (VIII B elements) surfaces, it is nontrivial to observe SERS signal of Py till a "borrowing SERS" strategy was independently developed by Leung and Weaver[19] and Fleischmann and Tian.[20] They deposited an ultrathin transition-metal layer over a SERS-active surface as new SERS substrates. With the aid of the long-range effect of EM enhancements created by the highly SERS-active substrate underneath, good-quality SERS spectra of adsorbates on several transition-metal films were obtained.[21] Recently, Tian and co-workers devised a series of methods of electrochemical treatment of electrode surfaces and chemical synthesis of nanoparticles to directly record good-quality SERS spectra from pure transition metals.[6,7,22] They have systematically investigated SERS of Py from transition-metal electrodes, such as iron, cobalt, nickel, ruthenium, rhodium, pallidium, and platinum.[23] Their studies revealed that Py's SERS spectral behavior on these metal surfaces was considerably different from that on the coinage metals. In addition to the difference in the overall SERS intensity due to different SERS activity of these metals, the relative intensities of different vibrations of Py were also found to be very sensitive to the nature of metal substrates.[7,24] For example, SERS spectra of Py adsorbed on these transition-metal surfaces showed that the signal of the υ_{12} vibration was weakened, but the Raman signals of the υ_{6a}, υ_{9a}, and υ_{8a} modes were enhanced significantly. This was particularly clear for Py adsorbed on iron, cobalt, nickel, and platinum.[25] For these metals, the Raman intensity of the 1596 cm^{-1} band of the υ_{8a} mode was comparable with that of the υ_1 mode. Because the Fermi level of the transition metals appears at the metal d bands, the electronic structures of the surface active sites become more complex than those of the coinage metals, and Py interacts with these metals much more strongly than the typical SERS substrates.[14,24] Therefore, it is desirable to give detailed theoretical calculations to interpret the spectral behavior on these metal electrodes.

SERS surface active sites, such as ad-atoms and ad-clusters of metal interacting with adsorbates, are an important concept to understand the chemical enhancement.[8] In contrast to the jellium[26] and dielectric models,[27] the cluster model of molecule-metal interfacial complexes can provide some key insights into the chemical bonding interaction and the charge-transfer mechanism in SERS processes.[11,28] The binding interaction leads to changes in the population of lone-pair electrons of the σ type and the delocalized molecular orbitals of the π type of the Py ring.[14,24,29−34] This results in not only the perturbation on geometries and vibrational fundamentals but also the changes of relative Raman intensities of the SERS spectra of Py.[14,32−36] In previous studies, cluster models combined with the density functional theory (DFT) were employed to explore the vibrational frequency shift of Py due to binding interactions with metal surfaces.[14,24,29−34] Cluster models were also used recently to predict the SERS spectra of Py interacting with copper, silver, and gold clusters,[18,35,36] and pyrazine[37] or pyrimidine[38] interacting with silver clusters. More recently, the time-dependent density functional theory (TD−DFT) method has been used to predict the dependence of SERS spectra on the incident wavelengths for Py interacting with silver and gold clusters.[11,39,40] It was found that the CT enhancement was about 10^3 for a Py−Ag_{20} complex, where the CT state was ascribed to a transition from a metal orbital to the $5\pi^*$ orbital of Py. To yield the strongest enhancement, an UV light was chosen to calculate the SERS spectra of Py−Ag_{20}.[11,40] Similarly, for the Py−Au_{20} complexes, resonance enhancements at 464 and 429 nm were calculated for vertical and surface complexes, respectively.[39] We believe that these incident photonic energies are too high such that interband transitions can be generally excited in the silver and gold clusters. In fact, the UV-SERS was only observed on the transition metals instead of the coinage metals.[23k] Accordingly, we paid our attention in this work to the influence of the charge-transfer mechanism on the dependence of the relative intensities of SERS spectra on the incident wavelengths. The relative long wavelengths to predict the frequency-dependent polarizability derivatives were chosen for this study.

The goal of the present work is to obtain a deeper insight into the chemical enhancement in Py adsorbed on different metal clusters (copper, silver, gold, and platinum). These clusters are analogies to SERS active centers. Our results show that the relative SERS intensities of a_1 modes of Py are sensitive to the binding interaction between Py and metal clusters, the nature of metal materials, and the incident wavelengths. Our results also demonstrate the reliability of DFT approaches to predict Raman spectra of free Py.

Computational Details

The cluster models used in the present work are shown in Figure 1. For M = copper, silver, gold, all nine configurations

have been explored. In Py−M_4(II) and Py−M_5(II) complexes, the planes of the Py ring and the metal cluster are chosen to be perpendicular to each other. Because Pt_5 prefers a 3D geometry of the square pyramid structure, only Py−M_5(III) and Py−M_5-(IV) types of geometries have been studied. These clusters are redefined as Py−Pt_5(I) and Py−Pt_5(II), respectively.

All of the quantum chemical calculations were obtained by using density functional theory (DFT) methods in the *Gaussian 03* package.[41] The DFT method in the flavor of B3LYP[42,43] was used for geometry optimizations and vibrational frequency calculations. The basis sets for carbon, nitrogen, and hydrogen atoms were 6-311+G**, which included a polarization function to all three atoms and a diffuse function to the carbon and nitrogen atoms. For all of the metal atoms, the valence electrons and the internal shells were described by the basis functions, LANL2DZ,[41] and the corresponding relativity effective core potentials.[44] In particular, to check the convergence of the basis sets in the prediction of Raman scattering intensities, larger basis sets, aug-cc-pVTZ and aug-cc-pVQZ,[45] were used for carbon, nitrogen, and hydrogen atoms in Py in selected clusters of PyM_2 and PyM_4. For free Py, MP2 and DFT calculations with the exchange-correlation functionals of B3PW91 (Perdew and Wang's 1991 gradient-corrected correlation functional)[46] and PBE1PBE (the 1997 hybrid functional of Perdew, Burke and Ernzerhof)[47] were also carried out.

On top of the optimized geometries, Raman intensities in on- and off-resonance Raman scattering processes were estimated in terms of the derivative of the polarizability with respect to a given normal coordinate. We employed the general formula in the harmonic approximation, where the differential Raman scattering cross section (DRSC) was given by,[48,49]

$$\left(\frac{d\sigma}{d\Omega}\right)_i = \frac{(2\pi)^4}{45} \cdot \frac{h}{8\pi^2 c\tilde{\nu}_i} \cdot \frac{(\tilde{\nu}_0 - \tilde{\nu}_i)^4}{1 - \exp(-hc\tilde{\nu}_i/k_B T)} S_i \quad (1)$$

$$S_i = 45\left(\frac{d\alpha}{dQ_i}\right)^2 + 7\left(\frac{d\gamma}{dQ_i}\right)^2 \quad (2)$$

Here, h, c, k_B, and T are the Planck constant, light speed, Boltzmann constant, and Kelvin temperature, respectively. $\tilde{\nu}_0$ and $\tilde{\nu}_i$ are the frequencies (in cm^{-1}) of incident light and the ith vibrational mode. S_i is the Raman scattering factor (in $Å^4$/amu) that can be directly calculated using the *Gaussian 03* program.[41] $d\alpha/dQ_i$ and $d\gamma/dQ_i$ are derivatives of isotropic and anisotropic polarizabilities with respect to a given normal coordinate, respectively. The frequency-dependent polarizabilities were calculated using the coupled perturbation methods.[50] Then, the polarizability derivatives were obtained by numerically differentiating the analytic polarizability with respect to nuclear coordinates.[51]

When the DRSC value of the Py molecule was measured in aqueous solutions,[57−60] the solvent effect can affect the Raman spectra of a polarizable molecule. Here, we used two models to include the solvent effect. The first one was the polarizable continuum model (PCM),[52] where we used the dielectric constant of water, $\epsilon_w = 78.39$ to calculate S_i. The second model was a hydrogen-bonded Py−W_3 cluster, with which we analyzed the influence of the solvent effect on the Raman bands of Py.[53]

Results and Discussion

A. Absolute DRSC of Free Pyridine. To evaluate SERS enhancement factors (EF), absolute Raman intensities of Py in gas or bulk phases have to be calculated as a reference. Figure 2 shows the simulated Raman spectra in the region of 500−3100 cm^{-1}. It is noted that Raman intensities of the C−H vibrations (~3100 cm^{-1}) were calculated to be stronger than those of the υ_1 and υ_{12} modes (~1000 cm^{-1}). This is, however, different from the Raman measurements, in which the Raman signals of the C−H stretching modes are slightly weaker than those of the υ_1 and υ_{12} bands.[15,16] The discrepancy between measured and simulated spectra was mainly from the lower response efficiency of the charge-coupled device and the light grating of Raman instruments in the high-frequency region rather than that in the middle frequency region.[54] For the υ_1 and υ_{12} modes, both MP2 and B3LYP results agree reasonably well with the observed Raman spectra. B3PW91 and PBE1PBE, on the other hand, predict the relative intensities of these two modes, which are in poor agreement with the experimental observations.[16,53]

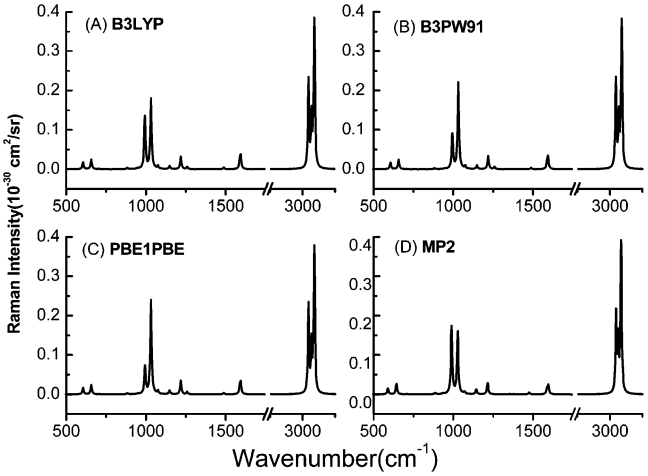

Figure 2. Simulated normal Raman spectra of Py at the incident wavelength of 514.5 nm with a Lorentzian line shape (a line width of 10 cm^{-1}) calculated with different theoretical methods of (A) B3LYP, (B) B3PW91, (C) PBE1PBE, and (D) MP2 with aug-cc-pVTZ basis set.

TABLE 1: Calculated Frequencies (in cm^{-1}) and Raman Activity (in $Å^4$/amu) of the Ring Breathing Mode (υ_1) and the Triangle Bending Mode (υ_{12}) for Free Pyridine

	6-311+G(d,p)		Aug-cc-pVTZ	
Method	$\upsilon_1(\omega_i/S_i)$	$\upsilon_{12}(\omega_i/S_i)$	$\upsilon_1(\omega_i/S_i)$	$\upsilon_{12}(\omega_i/S_i)$
MP2	1007.1/38.2	1043.2/29.8	1007.1/40.2	1046.5/36.7
B3LYP	1010.2/30.7	1046.6/34.4	1012.1/31.4	1051.3/41.6
B3PW91	1013.7/19.6	1049.0/43.8	1014.0/20.2	1052.7/51.4
PBE1PBE	1019.7/15.5	1055.3/48.4	1019.0/16.1	1058.3/55.9
B3LYP	1026.2/56.3	1049.1/17.0	1028.4/58.9	1053.5/21.9

Table 1 presents the vibrational frequencies and the corresponding S_i values calculated by using different methods. From Table 1, we see that the υ_{12} mode is more sensitive to the basis set quality than the υ_1 mode. Increasing the basis set from 6-311+G** to aug-cc-pVTZ results in average frequency shifts of 0.4 and 3.6 cm^{-1}, accompanied by a neat increase in the Raman activity by ~1.0 and 7.03 $Å^4$/amu for the υ_1 and υ_{12} modes, respectively. Hence, for B3LYP the 6-311+G** set may present an adequate basis set for the description of the υ_1 mode, though it is not yet converged for the υ_{12} mode. As we are more interested in the ratio of change of the Raman activity upon Py interaction with the metal, the basis set effect is expected to be smaller. 6-311+G** will be our basis set of choice for the study of the Py interaction with the metal clusters.

Table 2 summarizes the vibrational frequencies and DRSC values for the a_1 modes of free Py. In our previous study, we found that the SQMF-B3LYP method with the basis set of 6-311+G** reproduced well the vibrational frequencies of the

TABLE 2: Calculated and Experimental Differential Raman Scattering Cross-Section (in 10^{-30} cm^2/sr) and Scattering Factors (in Å^4/amu; in Parenthesis) with the Incident Wavelength of 514.5 nm for Selected a_1 Vibrational Modes of Pyridine

	Frequencies/cm^{-1}		Raman Intensity				
	expt.	B3LYP	B3LYP 6-311+G**	B3LYP aug-cc-pVTZ	B3LYP aug-cc-pVQZ	MP2 aug-cc-pVTZ	expt.[a]
υ_{6a}	601.2	605.8	0.45(3.9)	0.27(2.3)	0.27(2.3)	0.23(2.0)	
υ_1	991.4	998.5	2.09(30.7)	2.14(31.4)	2.26(33.1)	2.74(40.2)	(44)
υ_{12}	1031.7	1040.5	2.33(34.4)	2.81(41.6)	2.70(40.0)	2.48(36.7)	(35)
υ_{9a}	1218.0	1219.4	0.50(7.8)	0.51(7.9)	0.51(7.8)	0.46(7.1)	
υ_{8a}	1583.9	1594.4	0.41(14.0)	0.46(15.7)	0.47(15.8)	0.34(11.4)	

[a] Raman scattering factors of the υ_1 and υ_{12} modes were derived from ref 59.

TABLE 3: Calculated Raman Scattering Factors (Å^4/amu) and Differential Raman Scattering Cross Sections (10^{-30} cm^2/sr) of Selected a_1 Vibrational Modes of Pyridine and Py$-(H_2O)_3$ Using Different Solvation Models Combined with the B3LYP Method at an Incident Wavelength of 514.5 nm

	Py[a]				Py$-W_3$					
Species	6-311+G**		aug-cc-pVTZ		6-311+G**		aug-cc-pVTZ		aug-cc-pVTZ[a]	
mode	S_i	dσ/dΩ	S_i	dσ/dΩ	S_i	dσ/dΩ	S_i	dσ/dΩ	S_i	dσ/dΩ
υ_{6a}	10.8	1.26	5.7	0.66	2.4	0.28	1.5	0.17	4.3	0.50
υ_1	135.1	9.22	168.0	11.48	56.3	3.83	58.9	4.00	192.0	13.08
υ_{12}	114.1	7.72	118.1	8.00	17.0	1.15	21.9	1.48	76.1	5.15
υ_{9a}	13.5	0.88	12.9	0.83	7.2	0.46	7.14	0.46	15.4	1.00
υ_{8a}	68.2	2.02	75.7	2.25	15.2	0.37	12.9	0.38	67.0	1.98

[a] The results were calculated on the basis of the polarized continuum model.

a_1 modes for Py in the Ar matrix.[14,24,31] Hence, here we will only focus on DRSC and scattering factors. The corresponding DRSC values at different levels of theory are in concord with each other. All of the methods point out that the υ_1 and υ_{12} modes have the strongest Raman signals among others. We notice that B3LYP with three different basis sets all predicted that the υ_{12} mode possesses a higher Raman activity than the υ_1 mode. This is, however, contradictory to the result predicted by the MP2/aug-cc-pVTZ method. It seems that the B3LYP method has a tendency to slightly overestimate the Raman intensities of the low-intensity bands, like the υ_{6a}, υ_{9a}, and υ_{8a} bands. If the DRSC value of the υ_1 mode is taken as a reference, we can estimate that the ratios of the υ_{6a}, υ_{9a}, and υ_{8a} modes are about four times larger than the observed ratios.[56] Such a tendency is not alleviated by increasing the basis set from 6-311+G** to aug-cc-pVTZ. This may be attributed to the shortcoming of the B3LYP method, which underestimates the S_i value of the υ_1 mode. In terms of the Raman intensity of Py, MP2 is clearly superior to B3LYP, albeit it is much more expensive at the basis set of aug-cc-pVTZ.

Now, we will turn to a comparison of the calculated DRSC values with the experimental data to check the reliability of the MP2 and B3LYP methods. For Py, its Raman spectra have been measured in gas phases[57] and in the pure-liquid[58−60] and aqueous solutions.[59,60] These reported Raman spectra showed that the absolute and relative intensities depend on the excitation wavelengths, concentrations of aqueous solutions, and the chemical environments. The DRCS value of the υ_1 mode of Py measured at an excitation wavelength of 488.0 nm is about 1.51×10^{-29} cm^2/sr in its pure liquid.[58] According to the fourth power of the excitation frequency dependence, DRSC of the υ_1 mode decreases to 1.21×10^{-29} and 4.6×10^{-30} cm^2/sr at the incident wavelengths of 514.5 and 647.1 nm, respectively. These values are very close to 1.25×10^{-29} cm^2/sr for the excitation line at 514.5 nm in pure liquid[59] or 1.1×10^{-29} cm^2/sr for 514.5 nm and 4.2×10^{-30} cm^2/sr for 647.1 nm in aqueous solution.[60] This suggests that the Raman polarizability derivatives of the Py molecule have only a weak dependence on the incident wavelength in the long wavelength region of visible light. We also notice that these DRSC values are slightly larger than 6.4×10^{-30} cm^2/sr measured at the incident wavelength of 514.5 nm in gaseous phases.[57] Such a difference is probably due to the intermolecular interaction and the solvent effect. Our calculated numbers are 2.14×10^{-30} and 2.74×10^{-30} cm^2/sr at the levels of B3LYP/aug-cc-pVTZ and MP2/aug-cc-pVTZ, respectively, in general agreement with the experimental data. We also noted that a recently reported value ($\sim 10^{-31}$ cm^2/sr), calculated at the density functional level of BP86 (the gradient-corrected Becke−Perdew exchange-correlation functional) and adopted the incident wavelength of 514.5 nm,[11] is an order of magnitude smaller than our numbers reported here and, hence, is too small as compared to the experimental values.

Table 3 lists the Raman scattering factors (S_i) calculated with the PCM model to include the solvation effect. We used B3LYP combined with 6-311+G** and aug-cc-pVTZ basis sets. The PCM model effectively increases the DRSC value of the ν_1 model from 2.14×10^{-30} (gas phase) to 1.15×10^{-29} cm^2/sr (aqueous solutions) at the latter basis set. This aqueous number is in excellent agreement with the experimental data of 1.10×10^{-29} [59] or 1.25×10^{-29} cm^2/sr.[60] On the basis of the classical Onsager model, the solvent effect can be estimated from the factor $EF = [(n^2 + 2)/3]^4$, where n is the refractive index of the solvent. For pure Py liquids, n may be taken as 1.51, which leads to a 4.14-fold increase of EF due to the solvent effect.[61] Hence, B3LYP gives the DRSC value of the ν_1 model in the range of $8.7-9.4 \times 10^{-30}$ cm^2/sr for pure Py liquids. The corresponding MP2 value is 1.13×10^{-29} cm^2/sr. All of these numbers can be compared favorably with the observed value.[58−60]

To study how the hydrogen-bonded interaction between Py and water molecules will influence the Raman intensity, a Py−W_3 complex is used to calculate the S_i values. The results in Table 3 clearly show that the Raman intensity is not sensitive to the direct hydrogen bonding between Py and solvent. Instead, the long-range electrostatic interaction, as included in a PCM or Onsager model, plays an important role.

Figure 3 presents variations of the simulated Raman spectra of Py with the incident wavelengths. As can be seen, when the excitation wavelength moves from visible light to UV light, there are not only increases for the DRSC values of the a_1 modes, but also a enhanced Raman signal of the υ_{10a} mode. This υ_{10a}

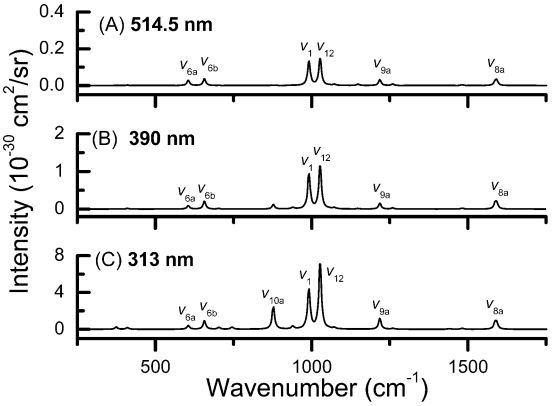

Figure 3. Dependence of the simulated preresonance Raman spectra of free Py upon the incident wavelengths. The incident wavelengths are (A) 514.5 nm, (B) 390 nm, and (C) 313 nm.

mode is an out-of-plane C−H bending vibration with a_2 symmetry, which can be interpreted by using the preresonance Raman scattering.[62] For free Py molecules, the first (S_1:$^1B_1$) and the second (S_2:$^1B_2$) singlet excited states have transition energies of 4.31 and 4.7 eV, which correspond to $n \rightarrow \pi^*$ and $\pi \rightarrow \pi^*$ transitions, respectively.[63] When the excitation line 325 nm (i.e., the photonic energy of 3.81 eV) is used, the preresonance Raman spectra can be observed.[62] The υ_{10a} mode is enhanced due to the vibronic coupling between the lowest two singlet excited states. This indicates that the preresonance Raman spectra should be predicted well on top of the DFT-coupled perturbation calculations. This encourages us to calculate the charge transfer state contributing to the CE enhancement when Py is adsorbed on metallic clusters.

B. Pyridine Interacting with the Copper, Silver, and Gold Clusters. On rough surfaces of coinage metals, the SERS signals can obtain a million-fold enhancement with respect to that of Py in the gas phase or the bulk.[10] In many cases, the EM enhancement plays an important role.[8] However, on smooth or low-index single-crystal surfaces, the EM enhancement is so small that it can be neglected. The DRSC values of the SERS vibrational mode of Py are enhanced mainly because of the CE mechanism. For Py adsorbed on a smooth Ag(100) surface in ultrahigh vacuum, Udagawa et al. reported a DRSC value of about 2.8×10^{-27} cm^2/sr for the υ_1 mode at an incident wavelength of 514.5 nm.[57] In this case, the EF was about 4.2×10^2 over the gaseous species. This was in contrast with an early result of Rowe et al., who claimed that the EF was less than 10^2.[64] Recently, Campion and Mullins obtained a DRSC value of only 5×10^{-29} cm^2/sr for the υ_1 mode of Py adsorbed on the low-index single-crystal surface of silver with an excitation wavelength of 514.5 nm in ultrahigh vacuum.[65] More recently, the SER spectra of Py adsorbed on copper and gold single-crystal surfaces have been obtained at the incident wavelength of 632.8 nm.[66,67] These studies showed that the EFs were not large, having numbers of 3 for Cu(100), 19 for Cu(111), 40 for Cu(110), and 1.0 to ~3.5 for Au(210), etc. To summarize these results, we conclude that the Raman intensities of Py are sensitive to the variation of the binding interaction between Py and different SERS substrates as well as the incident wavelength. To understand the influence of the two effects on Raman scattering intensity, we will calculate the static and preresonance Raman spectra. For static Raman spectra, we discuss the changes of S_i values with different complexes. Because the excitation by using the green laser at 514.5 nm will cause interband transitions, the SERS signals of Py adsorbed on copper or gold surfaces generally become very weak.[13,68−70] Therefore, we will consider the Raman intensity for the preresonance Raman spectra in the yellow light close to 632.8 nm.

Table 4 presents S_i values of Py−M$_n$ (M = copper, silver, and gold; n = 2−5) complexes calculated at the B3LYP/6-311+G**(C, N, H)/LANL2DZ(Cu, Ag, Au) level. Also presented in the parentheses are the ratios of the S_i values between Py−M$_n$ complexes and free Py. We may classify these complexes into three groups, depending on the interacting strengths between Py and M$_n$. Previously, we calculated that the binding energies for Py−Ag, Py−Ag$_4$(III), Py−Au, and Py−Au$_4$(III) were around 4.7, 5.4, 9.1, and 10.9 kcal/mol, respectively.[71] Such a weak binding interaction between Py and metal clusters may be considered as a physical adsorption state of Py on these metal clusters. This is mainly observed in the complexes of Py interacting with silver clusters and some nonactive sites of gold clusters. This kind of complex is labeled as the A-type. The A-type is characterized by a decrease in the ratio of the S_i values of the υ_{6a} mode, with one exception for complex Py−Au$_5$(II). There accompanies an increase of the ratios of the S_i values of the other modes. However, the weak binding interaction only leads to small changes in the Raman spectra. The largest ratio of the S_i value is 4.4 as found in the υ_{9a} mode of Py−Ag$_4$(I).

Recently, Schatz and co-workers have also studied the influence of the binding interaction on the Raman intensities of Py interacting with Ag$_2$ and Ag$_4$ clusters.[40] For Py−Ag$_2$ and Py−Ag$_4$(III), similar optimized structures were adopted. They calculated the Raman intensities of the υ_{8a} mode to be comparable to that of the υ_1 mode, whereas our predicted values are generally smaller for the former mode. This difference is probably due to the difference in the exchange-correlation functionals used, that is, B3LYP versus BP86.

The binding interaction increases in the second B-type, as compared to the A-type. In this case, the Raman activity of the υ_{12} mode obviously decreases. Their ratios of S_i values of υ_{12} are in a range within 0.0 to ~0.9. Meanwhile, the ratios of the S_i values between these complexes and free Py are generally smaller than 10, and there are three exception cases, which have larger ratios of 14.5 and 16.3 for the υ_{8a} mode of Py−Cu$_2$ and Py−Cu$_4$(III), respectively, as well as 15.9 for the υ_{9a} mode of Py−Cu$_5$ (I). The enhancements in Raman activities of υ_{6a}, υ_{9a}, and υ_{8a} modes depend on adsorption configurations of Py interacting with different metal clusters.

The third type, C-type, is characterized by a strong binding interaction between Py and metal clusters, and the significant enhancement of Raman signals of υ_{6a}, υ_1, υ_{9a}, and υ_{8a} modes can be observed in the this type of complexes. As compared to free Py, the S_i values of these modes increase significantly as shown in Table 4. On the basis of these static S_i values, the simulated normal Raman spectra are presented in Figure 4. For convenient comparisons, the simulated Raman spectra of selected complexes of other types, such as Py−Ag$_4$(I), Py−Cu$_4$(I), and Py−Au$_4$(I), are also presented in Figure 4. These results show that Raman intensities of these vibrations of Py are very sensitive to the adsorption configuration. Such an adsorption configuration can lead to the strongest peaks in a number of SERS spectra when Py adsorbs on these metal surfaces.[72−75]

The photon-induced charge-transfer mechanism is thought to contribute to the SERS spectral signal, which may change the relative Raman intensities of the different vibrational modes. Recently, TD−DFT studies have been used to predict the SERS spectra of Py interacting with silver and gold clusters.[11,39,40] They

TABLE 4: Raman Scattering Factors (in Units of Å⁴/amu) and the Relative Values (in Parentheses) with Respect to the Raman Scattering Factors of the Corresponding Vibrational Modes of Free Pyridine for Py−M_n (M = Cu, Ag, and Au; n = 2−5) Complexes Calculated at the B3LYP/6-311+G(C, N, H)/LANL2DZ(Cu, Ag, Au) Level**

metal	type	species	υ_{6a}	υ_1	υ_{12}	υ_{9a}	υ_{8a}
Ag_n	A	Py−Ag	2.5(0.6)	48.6(1.6)	41.7(1.2)	19.2(2.5)	21.8(1.6)
	A	Py−Ag_2	1.4(0.4)	50.1(1.6)	46.2(1.3)	11.6(1.5)	27.9(2.0)
	A	Py−Ag_3	3.1(0.8)	68.4(2.2)	37.0(1.1)	22.9(2.9)	28.3(2.0)
	A	Py−Ag_4(I)	1.2(0.3)	70.7(2.3)	34.5(1.0)	34.4(4.4)	19.8(1.4)
	C	Py−Ag_4(II)	157.0(40.4)	549.5(17.9)	20.6(0.6)	325.3(41.8)	1300.5(93.2)
	A	Py−Ag_4(III)	0.5(0.1)	43.5(1.4)	72.9(2.1)	23.4(3.0)	49.4(3.5)
	B	Py−Ag_5(I)	7.3(1.9)	83.6(2.7)	28.3(0.8)	76.8(9.9)	20.9(1.5)
	B	Py−Ag_5(II)	17.9(4.6)	108.8(3.5)	30.8(0.9)	43.5(5.6)	86.3(6.2)
	C	Py−Ag_5(III)	66.5(17.1)	297.5(9.7)	20.0(0.6)	107.2(13.8)	506.2(36.3)
	C	Py−Ag_5(IV)	44.4(11.4)	248.4(8.1)	18.7(0.5)	69.9(9.0)	327.3(23.4)
Cu_n	B	Py−Cu	13.7(3.5)	113.7(3.7)	13.8(0.4)	35.3(4.5)	96.2(6.9)
	B	Py−Cu_2	18.4(4.7)	164.8(5.4)	8.4(0.2)	29.6(3.8)	202.2(14.5)
	B	Py−Cu_3	18.1(4.6)	160.1(5.2)	1.5(0.0)	42.9(5.5)	128.7(9.2)
	B	Py−Cu_4(I)	11.8(3.0)	136.4(4.4)	3.0(0.1)	43.1(5.5)	80.3(5.7)
	C	Py−Cu_4(II)	348.4(89.6)	1322.9(43.1)	21.0(0.6)	956.3(122.8)	3415.4(244.7)
	B	Py−Cu_4(III)	15.7(4.0)	146.9(4.8)	18.4(0.5)	19.5(2.5)	227.5(16.3)
	B	Py−Cu_5(I)	13.8(3.5)	116.9(3.8)	8.2(0.2)	123.8(15.9)	43.5(3.1)
	C	Py−Cu_5(II)	58.4(15.0)	267.7(8.7)	5.6(0.2)	101.1(13.0)	390.2(27.9)
	C	Py−Cu_5(III)	194.2(49.9)	721.6(23.5)	18.7(0.5)	430.2(55.2)	1634.5(117.1)
	C	Py−Cu_5(IV)	254.8(65.5)	936.5(30.5))	29.9(0.9)	624.4(80.2)	2306.7(165.2)
Au_n	A	Py−Au	1.3(0.3)	37.6(1.2)	57.4(1.7)	10.3(1.3)	17.7(1.3)
	B	Py−Au_2	4.5(1.1)	117.4(3.8)	21.3(0.6)	13.8(1.8)	84.2(6.0)
	B	Py−Au_3	8.4(2.2)	122.9(4.0)	18.2(0.5)	10.9(1.4)	64.1(4.6)
	B	Py−Au_4(I)	4.0(1.0)	116.6(3.8)	16.7(0.5)	12.5(1.6)	41.6(3.0)
	C	Py−Au_4(II)	46.3(11.9)	293.1(9.6)	4.1(0.1)	95.9(12.3)	332.9(23.8)
	A	Py−Au_4(III)	2.8(0.7)	44.4(1.4)	104.2(3.0)	0.8(0.1)	43.5(3.1)
	A	Py−Au_5(I)	0.2(0.1)	69.7(2.3)	52.0(1.5)	24.5(3.1)	14.9(1.1)
	A	Py−Au_5(II)	4.8(1.2)	85.4(2.8)	43.7(1.3)	18.5(2.4)	38.6(2.8)
	C	Py−Au_5(III)	45.0(11.6)	290.9(9.5)	7.4(0.2)	79.9(10.3)	332.9(23.8)
	C	Py−Au_5(IV)	91.8(23.6)	491.7(16.0)	2.1(0.1)	210.6(27.0)	785.1(56.2)

found that the CT enhancement was about 10^3, in agreement with the experimental observation.[76] For Py-adsorbed silver surfaces, the EF in a magnitude of about 10^3 was also predicted.[77] In a special case of *p*-mercaptoaniline adsorbed on gold bowtie surfaces with a nanometer size, the EF due to the CT enhancement mechanism was found even up to 10^7.[78] Here, we pay our attention to the influence of the charge-transfer mechanism on the relative intensities of SERS spectra. Therefore, in our cases, the relatively long wavelengths are used in our calculations.

Figure 5 presents the simulated SERS spectra of Py−Ag_2 at the three different incident wavelengths. For this complex, we calculated that it has three lowest singlet excited states, such as S_1, S_2, and S_3 with transition energies of 2.09, 2.60, and 3.23 eV, respectively. The S_1 and S_2 states correspond to the CT excited states, that is, a symmetry-allowed transition from the highest occupied molecular orbital (HOMO) consisting of a silver 5s + 5s bonding orbital to the Py $4\pi^*$ orbital with b_1 symmetry and a symmetry-forbidden transition from the HOMO to a Py $5\pi^*$ orbital with a_2 symmetry. The third excited state having a large oscillator of 0.94 corresponds to a transition from the HOMO to an unoccupied orbital mainly consisting of the silver p_z orbital.

The calculated transition energy (2.09 eV) for S_1 is in agreement with the experimental observations.[76,79−81] For example, a similar value of 2.06 eV has also been determined from Py adsorbed on an evaporated silver film.[76] According to the Stokes and anti-Stokes Raman line intensity ratio in resonance Raman scattering, the charge transfer absorption band was determined to be 1.92 eV.[81] CT excitations of Py adsorbed on a Ag(111) surface have been observed by electron energy loss spectroscopy to be around 1.4 to ~2.4 eV.[79,80] An inverse photoemission experiment showed that the unoccupied $4\pi^*$ and $5\pi^*$ levels were around 2.9 ± 0.2 eV above the Fermi level on silver surfaces.[82]

To consider the influence of the CT mechanism in the Py−Ag_2 complex, three incident wavelengths, 640, 620, and 605 nm, have been used, which have energy gaps of 0.15, 0.09, and 0.04 eV, respectively, with respect to the S_1 transition energy of 2.09 eV, respectively. As seen in Figure 4, the relative Raman intensities of the simulated Raman spectra are sensitive to the incident wavelengths. Raman intensities of the υ_{8a} and υ_{9a} modes increase obviously with the incident photonic energy approaching the S_1 energy. In particular, the Raman intensities of these two modes surpass that of the υ_1 mode at 605 nm. On the contrary, the υ_{12} mode significantly decreases its Raman intensity. This is in line with our previous results and the other reported works.[18,83,84] In the S_1 state, the υ_{12} mode only has a small displacement of the equilibrium geometry with respect to that of the ground state, whereas the corresponding displacements of the υ_1, υ_{8a}, and υ_{9a} modes are more significant. Because there are no other states coupling to the S_1 state for Py−Ag_2, this simulated Raman spectrum is a typical one of Py.

The recent theoretical results calculated by Jensen et al. were quite different from ours reported here. They used a short incident wavelength of 376 nm (3.30 eV), which is close to the excitation to the S_3 excited state. As the S_3 state has a large oscillator strength, large electromagnetic resonance enhancement can be anticipated.[40] We are surprised to see that the 376 nm incident wavelength resulted in a large change in the relative Raman intensities in the SERS spectra. We suspect that their simulated Raman spectra were sensitive to the internal excitation of the metallic clusters. This idea will be further demonstrated in the later part of the present work.

For Py−Cu_2 and Py−Au_2, we do not present their simulated Raman spectra here. But we note that Py−Cu_2 has the S_1 CT state with the transition energy of 1.79 eV and a small oscillator strength of 0.0003. This calculated transition energy is in excellent agreement with 1.77 eV from the resonance Raman scattering,[82] but it is obviously too low as compared to 3.15

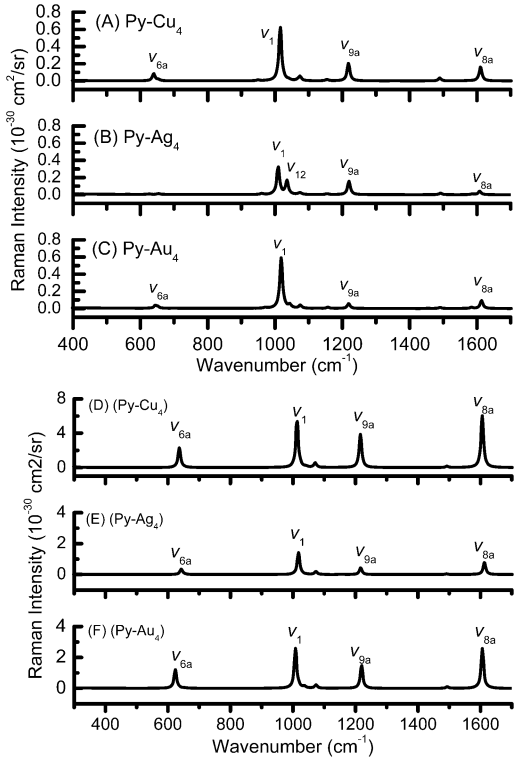

Figure 4. Simulated static Raman spectra of Py−M_4(I) and Py−M_4-(II) complexes (M = Cu, Ag, Au) at the B3LYP/aug-cc-pVTZ(C, N, H)/LanL2DZ (Cu, Ag, Au) level at the excitation line 514.5 nm for differential Raman scattering cross section in units 10^{-30} cm^2/sr and wavenumber in cm^{-1}. (A) Py−Cu_4(I), (B) Py−Ag_4(I), (C) Py−Au_4(I), (D) Py−Cu_4(II), (E) Py−Ag_4(II), and (F) Py−Au_4(II).

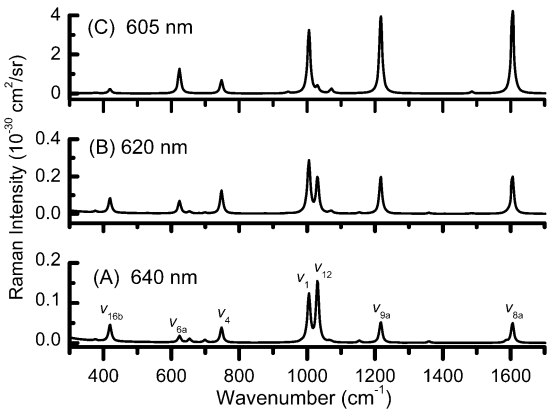

Figure 5. Simulated preresonance charge-transfer Raman spectra of Py−Ag_2 calculated with B3LYP/6-311+G(d,p) (C, N, H)/LANL2DZ-(Ag) at different excitation wavelengths of (A) 640 nm, (B) 620 nm, and (C) 605 nm.

and 3.75 eV from the two-photon photoemission spectroscopy.[85] For Py−Au_2, we calculate the transition energy to the S_1 state to be 2.87 eV. This is obviously too large as compared to 1.55 eV measured for the CT state of adsorbed Py on gold surfaces.[82] The TDDFT calculations predicted 2.0 eV for the S_1 CT state of Py−Au_{20}. [39]It is plausible that a too strong bonding HOMO orbital is formed in the small gold dimer, leading a too high transition energy for the S_1 state.

For Py−Cu_4 and Py−Ag_4, there are low-lying CT excited states, S_1 and S_2. The S_1 states, $^1A_2$, with transition energies of 1.50 and 1.67 eV for Py−Cu_4 and Py−Ag_4, respectively, are symmetry-forbidden. The S_1 states correspond to the transition from the HOMO orbital mainly consisting of the metal s orbital featured with a b_2 symmetry to the $4\pi^*(b_1)$ orbital of Py. The

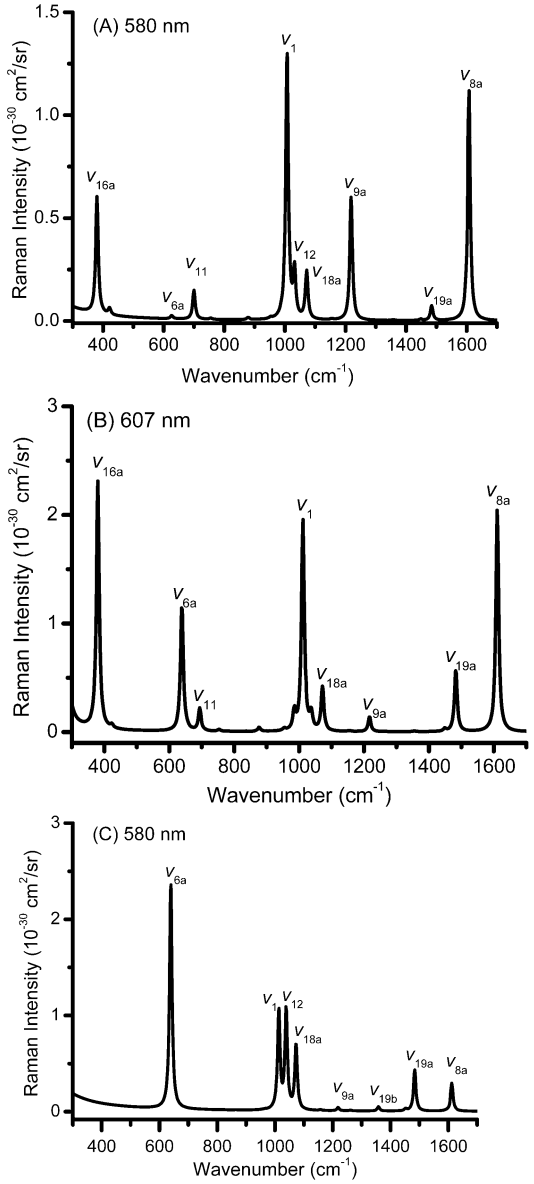

Figure 6. Simulated Raman spectra of Py interacting with the metal tetramer along a direction of the active site in a planar configuration. (A) Py−Ag_4(I), λ = 580 nm; (B) Py−Cu_4(I), λ = 607 nm; (C) Py−Cu_4(I), λ = 580 nm. Spectra have been broadened by a Lorentzian have a width of 10 cm^{-1}.

transition energies and oscillator strengths of the S_2 states ($^1B_1$) are 2.12 eV and 0.0008, and 2.22 eV and 0.0006 for Py−Cu_4 and Py−Ag_4, respectively.[71] The incident wavelengths we chose are 607 nm (2.04 eV) and 580 nm (2.14 eV), for Py−Cu_4 and Py−Ag_4, respectively. Hence, for both clusters, the gaps between the incident wavelengths and the transition energy state of S_2 are the same (0.08 eV). For Py−Au_4, there are five low-lying excited states (ΔE_{S1} = 2.25 eV, f_{S1} = 0.0145; ΔE_{S2} = 2.45 eV, f_{S2} = 0.0; ΔE_{S3} = 2.80 eV, f_{S3} = 0.0011; ΔE_{S4} = 3.09 eV, f_{S4} = 0.4639; and ΔE_{S5} = 3.10 eV, f_{S3} = 0.0003). Among them, only S_2 and S_5 belong to the CT excited states. Because the S_2 state is symmetry-forbidden and the S_5 state has a too large transition energy, we decided to check the influence of the excited state on the Raman spectrum of Py−Au_4 by considering the incident wavelength of 580 nm (2.14 eV) close to the S_1 state. The S_1 state is mainly from a transition within the Au_4 cluster itself. Its transition energy (2.25 eV) is close to the plasmon resonance peak at about 520 nm (2.38 eV) from isolated golden nanoparticles.[86]

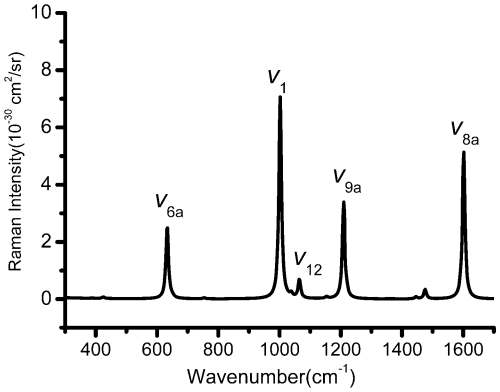

Figure 7. Simulated static Raman spectrum of the Py−Pt_5 complex calculated at the B3LYP/6-311+G(d,p) (C, N, H)/Lanl2DZ level with an incident wavelength of 514.5 nm.

Figure 6 presents the simulated Raman spectra for the Py−M_4(I) complexes (M = Cu, Ag, Au). As seen in part A of Figure 6 for Py−Ag_4(I), the Raman bands of υ_1, υ_{8a}, and υ_{9a} modes exhibit a significant enhancement effect due to the charge-transfer mechanism. In contrast to the Raman spectra in part A of Figure 4, the Raman intensities of the υ_{8a} and υ_{9a} modes become comparable to the υ_1 mode, whereas the enhancement effect is small for the υ_{6a} mode. This can be understood using the Raman Franck−Condon factors of these three vibrational modes. It is well known that a large normal mode displacement causes a significant enhancement in Raman signals. For the three modes, their displacements are $\upsilon_{8a} > \upsilon_{9a} > \upsilon_{6a}$,[18] in agreement with the results based on the free Py and its anionic radical.[84] It shall be noted that the ring twist mode (υ_{16a}) with a Raman band at 380 cm^{-1} also exhibits a significant enhancement when the CT state is excited. This mode has an a_2 symmetry, and there exists a vibronic coupling between the S_2 (B_1) and S_3 (B_2) states through the υ_{16a} mode. Additionally, the υ_{16a} mode involves motions of the atoms closely associated with the π^* (a_2) orbital, similar to the Raman intensity enhancement of the υ_{10a} in free Py.[11,62] Although Zhao et al. have also considered the CT state,[11] the relative Raman intensities in their simulated Raman spectrum are slightly different from ours present here. The difference comes possibly from two aspects. First, Zhao et al.[11] calculated the resonance Raman spectra, whereas we calculate the preresonance Raman. Second, the different size of the metallic clusters and different theoretical methods were used.

Part B of Figure 6 clearly shows the metallic effect in the simulated Raman spectrum of Py−Cu_4(I). In contrast to that of Py−Ag_4, the υ_{9a} mode in Py−Cu_4 is not enhanced, whereas the υ_{6a} mode exhibits a strong Raman peak. Here, the vibronic coupling results in a significant enhancement effect on the υ_{16a} mode, although it is likely that the Raman intensity of the υ_{16a} mode is overestimated.

The simulated Raman spectrum presented in part C of Figure 6 gives rise from an internal excitation within the Au_4 cluster itself. The predicted spectrum is different from the static Raman spectrum shown in part C of Figure 4. A comparison of both predicted spectra shows that the relative Raman intensities of different a_1 vibrational modes are very sensitive to the metal electron excitation. The υ_{6a} mode exhibits a large enhancement effect as compared with the υ_1, υ_{8a}, and υ_{9a} modes. This is understandable, as the electronic excitation of a metal active SERS site can directly influence the relative Raman intensities. This is different from the surface plasmon resonance of collective excitations of delocalized electrons, which yields the same enhancement effect on the vibrational modes with the same irreducible representation.

C. Pyridine Interacting with the Pt_5 Clusters. The EM enhancement is unexpected to change the relative Raman intensities of the a_1 modes of Py.[2] Additionally, the EM enhancement is not too sensitive to the excitation wavelengths for the same transition-metal substrate.[87,88] The change in relative intensities for different a_1 modes of Py adsorbed on platinum surfaces is anticipated to arise from the chemical bonding interaction and the charge-transfer mechanism.[23,89−91] Figure 7 presents the static Raman spectrum at the incident wavelength of 514.5 nm. We find that the Raman peaks of the υ_{8a} and υ_{9a} modes are enhanced as a result of the chemical bonding interaction, whereas the Raman peak of the υ_{12} mode is decreased with respect to the intensity of the υ_1 mode. Taking the Raman intensities of free Py as references, we can obtain the EFs for the selected a_1 modes as shown in Table 5. Significantly, the chemical bonding causes an enhancement on the υ_{8a} and υ_{9a} modes larger than 100 folds of free Py. This enhancement is comparable with the CT enhancement, which is often considered as the major contribution of the CE enhancement. In contrast to the CT enhancements of Py adsorbed on coinage metals[66,67,76,77] and cobalt,[7,92] we conclude that the binding interaction can be a very important factor in analyzing the SERS enhancement for Py binding to platinum.

Experiments show that the CT mechanism takes effect as the incident radiation energy matches the energy of an excited CT state for Py adsorbed on the platinum electrodes. For the Py−Pt_5(I) complex, the TD-B3LYP calculation predicted 140 vertical excited states, which are in a narrow range of transition energies from 0.2 to 3.0 eV with respect to that of the ground electronic state. Among all of these excited states, we found three excited states with oscillator strengths larger than 0.03. The other excited states have an oscillator strength smaller than 0.01. The TD-B3LYP calculations predict that the first CT state lies at 2.09 eV with $f = 0.0417$. Such an excited state is attributed to a transition from a platinum d orbital to the $4\pi^*$ (b_1) HOMO of the Py ring. The second state, consisting of two main components (~20% from the CT excitation and ~80% from metal internal excitations), is at 2.34 eV with $f = 0.0309$. The third

TABLE 5: Calculated Frequencies (Units in cm^{-1}), Raman Scattering Factors (S_i, Units in $Å^4$/amu), Differential Raman Scattering Cross-Section ($d\sigma/d\Omega$, Units in 10^{-30} cm^2/sr), Enhancement Factors (EF) of Total Symmetric Vibrations of Py−Pt_5 Complexes at the Level of B3LYP/6-311+G(C, N, H)/LANL2DZ(Pt)[a]**

	Frequency		Py−Pt_5(I)		Py−Pt_5(II)		
Mode	expt.[b]	theory	S_i	$d\sigma/d\Omega$	S_i	$d\sigma/d\Omega$	EF
υ_{6a}	636	633.4	348.11	40.04	361.83	41.61	~90
υ_1	1011	1002.0	1625.12	110.57	1733.08	117.92	~50
υ_{12}	1037	1038.5	28.47	1.92	31.75	2.14	~1
υ_{9a}	1208	1209.3	831.77	53.82	899.57	58.21	>100
υ_{8a}	1591	1601.2	2746.17	81.24	2934.85	86.83	~200

[a] The DRSC values are calculated at the incident wavelength of 514.5. The enhanced factor is estimated as a ratio between the DRSC values of the same vibrational modes in Py−Pt_5 and free pyridine. [b] Observed frequencies are extracted from ref 91.

state is a CT excited state, which is contributed by a transition with a component more than 80%. Besides the above three excited states, there are many transition-allowed states, which more or less contain some CT components.

We note that the chemical enhancement is generally larger from the interaction of Py with transition metals than coinage metals. However, an intense Raman signal is only observed for Py adsorbed on coinage metals. This is due to the fact that the electromagnetic enhancement makes a dominant contribution for coinage metals. However, the relative SERS intensities depend on the binding interaction rather than the electromagnetic enhancement, suggesting that there exists a metal-dependent behavior of SERS spectra for the a_1 modes on metal surfaces. Therefore, to estimate the chemical effect, due to chemical bondings, on the Raman signals of various modes is very important for a deep understanding of SERS spectra for Py adsorbed on transition-metal electrodes.

Conclusions

We have investigated the influence of the binding interaction and the charge-transfer mechanism on the Raman intensities of several a_1 vibrational modes of Py interacting with copper, silver, gold, and platinum metals. In the present work, we present DFT results for understanding the dependence of metals and excitation wavelengths on the SERS intensities. The analysis is on the basis of a well-known concept that the electromagnetic enhancement yields the same enhancement effect on the vibrational modes with the same irreducible representation, for example, the a_1 mode of adsorbed Py molecules.

The chemical enhancement can be divided in detail into two enhancement mechanisms, that is, the chemical bonding effect and the charge-transfer mechanisms. Both chemical enhancement mechanisms have a synergetic effect to the relative intensities of the υ_{6a}, υ_{8a}, and υ_{9a} modes comparable to that of the υ_1 mode for Py adsorbed on metal surfaces. This could be a reliable interpretation for SERS observations that the four normal modes generally have strong Raman signals. In contrast to coinage metals, the chemical bonding interaction is stronger in the Py/Pt system, suggesting that the SERS enhancement caused by chemical bonding is essential in comprehensively analyzing the SERS spectra of Py adsorbed on transition-metal surfaces. The charge-transfer mechanism depends on the electronic structure of SERS active centers and the metal materials, the property of charge transfer states, and the excitation wavelengths. The intensities of some other vibrational modes are enhanced and are closely associated with the large displacement at two related potential energy surfaces. To gain a clear understanding of the changes of the relative SERS intensities of Py adsorbed on different metals, it is necessary to experimentally characterize the electronic structure of the surface adsorption site and to further analyze theoretically the surface excited states. On the basis of the preresonance Raman scattering processes, useful information can be obtained for the CT mechanism of Py adsorbed on the metal surfaces.

Acknowledgment. This work is supported by the Natural Science Foundation of China (Grants 10474082, 20573087, and 20433040) and Ministry of Science and Technology (973 Program No. 2007CB815303). The partial calculations are completed at the high performance computational centre of Xiamen University and the national high performance computational centre of Taiwan.

References and Notes

(1) Chang, R. K.; Furtak, T. E. *Surface Enhanced Raman Scattering*; Plenum Press: New York, 1982.
(2) Moskovits, M. *Rev. Mod. Phys.* **1985**, *57*, 783−826.
(3) Campion, A.; Kambhampati, P. *Chem. Soc. Rev.* **1998**, *27*, 241−250.
(4) Nie, S. M.; Emery, S. R. *Science* **1997**, *275*, 1102−1106.
(5) Kneipp, K.; Wang, Y.; Kneipp, H.; Perelman, L. T.; Itzkan, I.; Dasari, R.; Feld, M. S. *Phys. Rev. Lett.* **1997**, *78*, 1667−1670.
(6) Tian, Z. Q.; Ren, B. *Annu. Rev. Phys. Chem.* **2004**, *55*, 197−229.
(7) Tian, Z. Q.; Ren, B.; Wu, D. Y. J. *Phys. Chem. B* **2002**, *106*, 9463−9483.
(8) Otto, A.; Mrozek, I.; Grabhorn, H.; Akemann, W. *J. Phys. Condens. Matter* **1992**, *4*, 1143−1212.
(9) Fleischmann, M.; Hendra, P. J.; McQuillan, A. J. *Chem. Phys. Lett.* **1974**, *26*, 163.
(10) Jeanmaire, D. J.; Van Duyne, R. P. *J. Electroanal. Chem.* **1977**, *84*, 1−17.
(11) Zhao, L.; Jensen, L.; Schatz, G. C. *J. Am. Chem. Soc.* **2006**, *128*, 2911−2919.
(12) Angel, S. M.; Katz, L. F.; Archbald, D. D.; Lin, L. T.; Honigs, D. E. *Appl. Spectrosc.* **1988**, *42*, 1327−1331.
(13) Gao, J. S.; Tian, Z. Q. *Chem. Phys. Lett.* **1996**, *262*, 151−154.
(14) Wu, D. Y.; Ren, B.; Jiang, Y. X.; Xu, X.; Tian, Z. Q. *J. Phys. Chem. A* **2002**, *106*, 9042−9052.
(15) Klots, T. D. *Spectrochim. Acta, Part A* **1998**, *54*, 1481−1498 and references therein.
(16) Urena, F. P.; Gomez, M. F.; Gonzalez, J. J. L.; Torres, *Spectrochim. Acta, Part A* **2003**, *59*, 2815−2839.
(17) Birke, R. L.; Lombardi, J. R. in *Spectroelectrochemistry-Theory and Practice*; Gale R. J., Ed.; Plenum Press: New York, 1988; pp 263.
(18) Wu, D. Y.; Hayashi, M.; Lin, S. H.; Tian, Z. Q. *Spectrochim. Acta A* **2004**, *60*, 137−146.
(19) Leung, L. W. H.; Weaver, M. J. *J. Electroanal. Chem.* **1987**, *217*, 367−384.
(20) Fleischmann, M.; Tian, Z. Q. *J. Electroanal. Chem.* **1987**, *217*, 385−395.
(21) Zou, S.; Weaver, M. J. *Anal. Chem.* **1998**, *70*, 2387−2397.
(22) Tian, Z. Q.; Ren, B.; Mao, B. W. *J. Phys. Chem. B* **1997**, *101*, 1338−1346.
(23) (a) Cao, P. G.; Yao, J. L.; Ren, B.; Mao, B. W.; Gu, R. A.; Tian, Z. Q. Chem. Phys. Lett. **2000**, *316*, 1−5. (b) Gu, R. A.; Cao, P. G.; Yao, J. L.; Ren, B.; Xie, Y.; Mao, B. W.; Tian, Z. Q. *J. Electroanal. Chem.* **2001**, *505*, 95−99. (c) Wu, D. Y.; Xie, Y.; Ren, B.; Yan, J. W.; Mao, B. W.; Tian, Z. Q. *Phys. Chem. Comm.* **2001**, *18*. (d) Xie, Y.; Wu, D. Y.; Liu, G. K.; Huang, Z. F.; Ren, B.; Yan, J. W.; Yang, Z. L.; Tian, Z. Q. *J. Electroanal. Chem.* **2003**, *554*−*555*, 417−425. (e) Ren, B.; Huang, Q. J.; Cai, W. B.; Mao, B. W.; Liu, F. M.; Tian, Z. Q. *J. Electroanal. Chem.* **1996**, *415*, 175−178. (f) Huang, Q. J.; Lin, X. F.; Yang, Z. L.; Hu, J. W.; Tian, Z. Q. *J. Electroanal. Chem.* **2004**, *563*, 121−131. (g) Gu, R. A.; Shen, X. Y.; Yan, J. W.; Mao, B. W.; Tian, Z. Q. *J. Phys. Chem. B* **2004**, *108*, 17519−17522. (h) Gao, J. S.; Tian, Z. Q. *Spectrochim. Acta A* **1997**, *53*, *1595*−*1600.* (i) Ren, B.; Lin, X. F.; Jiang, Y. X.; Mao, B. W.; Tian, Z. Q. *J. Phys. Chem. B* **2003**, *107*, 899−902. (j) Cai, W. B.; She, C. X.; Ren, B.; Yao, J. L.; Tian, Z. W.; Tian, Z. Q. *J. Chem. Soc., Faraday Trans.* **1998**, *94*, 3127−3133. (k) Ren, B.; Lin, X. F.; Yang, Z. L.; Liu, G. K.; Aroca, R. F.; Mao, B. W.; Tian, Z. Q. *J. Am. Chem. Soc.* **2003**, *125*, 9598−9599.
(24) Wu, D. Y.; Ren, B.; Xu, X.; Liu, G. K.; Yang, Z. L.; Tian, Z. Q. *J. Chem. Phys.* **2003**, *119*, 1701−1709.
(25) Wu, D. Y.; Ren, B.; Tian, Z. Q. *Isr. J. Chem.* **2006**, *46*, 317−327.
(26) Xu, M.; Dignam, M. J. *J. Chem. Phys.* **1992**, *96*, 8000−8011.
(27) Corni, S.; Tomasi, J. *J. Chem. Phys.* **2002**, *116*, 1156−1164.
(28) Nakai, H.; Nakatsuji, H. *J. Chem. Phys.* **1995**, *103*, 2286−2294.
(29) Arenas, J. F.; Lopez-Tocon, I.; Castro, S. P.; Lopez-Ramirez, M. R.; Otero, J. C. *J. Raman Spectrosc.* **2005**, *36*, 515−521.
(30) Vivoni, A.; Birke, R. L.; Foucault, R.; Lombardi, J. R. *J. Phys. Chem. B* **2003**, *107*, 5547−5557.
(31) Wu, D. Y.; Hayashi, M.; Shiu, Y. J.; Liang, K. K.; Chang, C. H.; Yeh, Y. L.; Lin, S. H. J. *Phys. Chem. A* **2003**, *107*, 9658−9667.
(32) Johansson, P. *Phys. Chem. Chem. Phys.* **2005**, *7*, 475−482.
(33) Muniz-Miranda, M.; Cardini, G.; Schettino, V. *Theor. Chem. Acc.* **2004**, *111*, 264−269.
(34) Cardini, G.; Muniz-Miranda, M.; Paglial, M.; Schettino, V. *Theor. Chem. Acc.* **2007**, *117*, 451−458.
(35) Wu, D. Y.; Duan, S.; Ren, B.; Tian, Z. Q. *J. Raman Spectrosc.* **2005**, *36*, 533−540.
(36) Wu, D. Y.; Ren, B.; Tian, Z. Q. *Chem. Phys. Chem.* **2006**, *7*, 619−628.
(37) Arenas, J. F.; Soto, J.; Tocon, I. L.; Fernandez, D. J.; Otero, J. C.; Marcos, J. I. *J. Chem. Phys.* **2002**, *116*, 7207−7216.
(38) Centeno, S. P.; Lopez-Tocon, I.; Arenas, J. F.; Soto, J.; Otero, J. C. *J. Phys. Chem. B* **2006**, *110*, 14916−14922.
(39) Aikens, C. M.; Schatz, G. C. *J. Phys. Chem. A* **2006**, *110*, 13317−13324.
(40) Jensen, L.; Zhao, L. L.; Schatz, G. C. *J. Phys. Chem. C* **2007**, *111*, 4756−4764.

(41) Frisch, M. J.; Trucks, G. W.; Schlegel, H. B.; Scuseria, G. E.; Robb, M. A.; Cheeseman, J. R.; Montgomery, J. A., Jr.; Vreven, T.; Kudin, K. N.; Burant, J. C.; Millam, J. M.; Iyengar, S. S.; Tomasi, J.; Barone, V.; Mennucci, B.; Cossi, M.; Scalmani, G.; Rega, N.; Petersson, G. A.; Nakatsuji, H.; Hada, M.; Ehara, M.; Toyota, K.; Fukuda, R.; Hasegawa, J.; Ishida, M.; Nakajima, T.; Honda, Y.; Kitao, O.; Nakai, H.; Klene, M.; Li, X.; Knox, J. E.; Hratchian, H. P.; Cross, J. B.; Bakken, V.; Adamo, C.; Jaramillo, J.; Gomperts, R.; Stratmann, R. E.; Yazyev, O.; Austin, A. J.; Cammi, R.; Pomelli, C.; Ochterski, J. W.; Ayala, P. Y.; Morokuma, K.; Voth, G. A.; Salvador, P.; Dannenberg, J. J.; Zakrzewski, V. G.; Dapprich, S.; Daniels, A. D.; Strain, M. C.; Farkas, O.; Malick, D. K.; Rabuck, A. D.; Raghavachari, K.; Foresman, J. B.; Ortiz, J. V.; Cui, Q.; Baboul, A. G.; Clifford, S.; Cioslowski, J.; Stefanov, B. B.; Liu, G.; Liashenko, A.; Piskorz, P.; Komaromi, I.; Martin, R. L.; Fox, D. J.; Keith, T.; Al-Laham, M. A.; Peng, C. Y.; Nanayakkara, A.; Challacombe, M.; Gill, P. M. W.; Johnson, B.; Chen, W.; Wong, M. W.; Gonzalez, C.; Pople, J. A. *Gaussian 03*, revision C.02; Gaussian, Inc.: Wallingford, CT, 2004.

(42) (a) Becke, A. D. *J. Chem. Phys.* **1993**, *98*, 5648. (b) Lee, C.; Yang, W.; Parr, R. G. *Phys. Rev. B* **1988**, *37*, 785.

(43) (a) Hay, P. J.; Wadt, W. R. *J. Chem. Phys.* **1985**, *82*, 270. (b) Wadt, W. R.; Hay, P. J. *J. Chem. Phys.* **1985**, *82*, 284. (c) Hay, P. J.; Wadt, W. R. *J. Chem. Phys.* **1985**, *82*, 299.

(44) (a) Hay, P. J.; Wadt, W. R. *J. Chem. Phys.* **1985**, *82*, 270. (b) Wadt, W. R.; Hay, P. J. *J. Chem. Phys.* **1985**, *82*, 284. (c) Hay, P. J.; Wadt, W. R. *J. Chem. Phys.* **1985**, *82*, 299.

(45) Woon, D. E.; Dunning, T. H., Jr. *J. Chem. Phys*. **1993**, *98*, 1358.

(46) (a) Perdew, J. P.; Burke, K.; Wang, Y. *Phys. Rev. B* **1996**, *54*, 16533. (b) Perdew, J. P. In *Electronic Structure of Solids 91*; Ziesche, P., Eschrig, H., Eds.; Akademie Verlag: Berlin, 1991; p 11.

(47) Perdew, J. P.; Burke, K.; Ernzerhof, M. *Phys. Rev. Lett.* **1996**, *77*, 3865.

(48) Long, D. A. *Raman Spectroscopy*; McGraw-Hill: New York, 1977.

(49) Neugebauer, J.; Reiher, M.; Kind, C.; Hess, B. A. *J. Comput. Chem.* **2002**, *23*, 895−910.

(50) Bauernschmitt, R.; Ahlrichs, R. *Chem. Phys. Lett*. **1996**, *256*, 454.

(51) Dykstra, C. E.; Jasien, P. G. *Chem. Phys. Lett.* **1984**, *109*, 388.

(52) Cappelli, C.; Corni, S.; Tomasi, J. *J. Chem. Phys.* **2001**, *115*, 5531−5535.

(53) Schlucker, S.; Singh, R. K.; Asthana, B. P.; Popp, J.; Kiefer, W. *J. Phys. Chem. A* **2001**, *105*, 9983−9989.

(54) McCreery, R. L. *Raman Spectroscopy for Chemical Analysis*; Wiley: New York, 2000; pp 251−291.

(55) Koch, W.; Holthausen, M. C. *A Chemist's Guide to Density Functional Theory*, 2nd ed.; Wiley-VCH: New York, 2001; pp 177−195

(56) Schrader, B. *Raman/Infrared Atlas of Organic Compounds*, 2nd ed.; VCH: Weinheim, Germany 1989, I7-01.

(57) Udagawa, M.; Chou, C. -C.; Hemminger, J. C.; Ushioda, S. *Phys. Rev. B* **1981**, *23*, 6843−6846.

(58) Skinner, J. G.; Nilsen, W. G. *J. Opt. Soc. Am.* **1968**, *58*, 113−119.

(59) Mierecki, R. *J. Raman Spectrosc.* **1986**, *17*, 35−38.

(60) Weaver, M. J.; Farquharson, S.; Tadayyoni, M. A. *J. Chem. Phys.* **1982**, *82*, 4867−4874.

(61) (a) Schrotter, H. W.; Klockner, H. W. In *Raman Spectroscopy of Gases and Liquids*; Weber, A., Ed.; Springer: Berlin, 1979; p 123. (b) Weast, R. C. *CRC Handbook of Chemistry and Physics*; 1970−1971; p e229.

(62) Mochizuki, Y.; Kaya, K.; Ito, M. *J. Chem. Phys.* **1976**, *65*, 4867−4874.

(63) Cai, Z. L.; Reimers, J. R. *J. Phys. Chem. A* **2000**, *104*, 8389−8408.

(64) Rowe, J. E.; Shank, C. V.; Zwemer, D. A.; Murray, C. A. *Phys. Rev. Lett.* **1980**, *44*, 1770−1773.

(65) Compion, A.; Mullins, D. R. *Chem. Phys. Lett.* **1983**, *94*, 576−.

(66) Brolo, A. G.; Irish, D. E.; Lipkowski, J. *J. Phys. Chem. B* **1997**, *101*, 3906−3909.

(67) Bruckbauer, A.; Otto, A. *J. Raman Spectrosc.* **1998**, *29*, 665−672.

(68) Ren, B.; Lin, X. F.; Jiang, Y. X.; Cao, P. G.; Xie, Y.; Huang, Q.; Tian, Z. Q. *Appl. Spectrosc.* **2003**, *57*, 419−427.

(69) Messinger, B. J.; von Raben, K. U.; Chang, R. K.; Barber, P. W. *Phys. Rev. B* **1981**, *24*, 649−657.

(70) Otto, A. *Light Scattering in Solid*, vol. IV; Cardona, M., Guntherodt, G. Eds.; Springer-Verlag, Berlin, 1984; pp 289−418.

(71) Wu, D. Y.; Hayashi, M.; Chang, C. H.; Liang, K. K.; Lin, S. H. *J. Chem. Phys.* **2003**, *118*, 4073−4085.

(72) Kudelski, A.; Bukowska, J.; Janik-Czachor, M.; Grochala, W.; Szummer, A.; Dolata, M. *Vib. Spectrosc*. **1998**, *16*, 21−29.

(73) Allen, C. S.; Schatz, G. C.; van Duyne, R. P. *Chem. Phys. Lett.* **1980**, *75*, 201−205.

(74) Creighton, J. A. *Surf. Sci.* **1986**, *173*, 665−672.

(75) Zou, C.; Jagodzinski, P. W. *J. Phys. Chem. B* **2005**, *109*, 1788−1793.

(76) Yamada, H.; Nagata, H.; Toba, K.; Nakao, Y. *Surf. Sci*. **1987**, *182*, 269−286.

(77) Persson, B. N. J. *Chem. Phys. Lett.* **1981**, *82*, 561−565.

(78) Fromm, D. P.; Sundaramurthy, A.; Kinkhabwala, A.; Schuck, P. J.; Kino, G. S.; Moerner, W. E. *J. Chem. Phys.* **2006**, *124*, 061101.

(79) Schmeisser, D.; Demuth, J. E. Avouris Ph. *Chem. Phys. Lett*. **1981**, *87*, 324−326.

(80) Demuth, J. E.; Sanda, P. N. *Phys. Rev. Lett.* **1981**, *47*, 57−60.

(81) Marinyuk, V. V.; Lazorenko-Manevich, R. M.; Kolotyrkin, Y. M. *J. Electroanal. Chem.* **1980**, *110*, 111−118.

(82) Otto, A.; Frank, K. H.; Reihl, B. *Surf. Sci*. **1985**, *163*, 140−152.

(83) Lee, M. T.; Wu, D. Y.; Tian, Z. Q.; Lin, S. H. *J. Chem. Phys.* **2005**, *99*, 094719.

(84) Arenas, J. F.; Lopez-Tocon, I.; Otero, J. C.; Marcos, J. I. *J. Phys. Chem.* **1996**, *100*, 9254−9261 and references therein.

(85) Zhong, Q.; Gahl, C.; Wolf, M. *Surf. Sci.* **2002**, *496*, 21−32.

(86) Lee, K. S.; El-Sayed, M. A. *J. Phys. Chem. B* **2005**, *109*, 20331−20338.

(87) Cline, M. P.; Barber, P. W.; Chang, R. K. *J. Opt. Soc. Am. B* **1986**, *3*, 15−21.

(88) Tian, Z. Q.; Yang, Z. L.; Ren, B.; Li, J. F.; Zhang, Y.; Hu, J. W.; Wu, D. Y. *Faraday Discuss.* **2005**, *132*, 159−170.

(89) Bilmes, S. A.; Rubim, J. C.; Otto, A.; Arvia, A. J. *Chem. Phys. Lett.* **1989**, *159*, 89−96.

(90) Tian, N.; Zhou, Z. Y.; Sun, S. G.; Cui, L.; Ren, B.; Tian, Z. Q. *Chem. Comm*. **2006**, 4090−4092.

(91) Ren, B.; Wu, D. Y.; Tian, Z. Q. *In-Situ Spectroscopic Studies of Adsorption at the Electrode and Electrocatalysis*, Chap. 10; Sun, S. G., Christensen, P. A., Wieckowski, A., Eds.; Elsevier: Amsterdam, 2007; pp 299−337.

(92) Xie, Y.; Wu, D. Y.; Liu, G. K.; Huang, Z. F.; Ren, B.; Yan, J. W.; Yang, Z. L.; Tian, Z. Q. *J. Electrochem. Chem*. **2003**, *554*, 417−425.